Silver and Copper Nitride Cooperate for CO Electroreduction to Propanol

Hong Phong Duong, Jose Guillermo Rivera de la Cruz, Ngoc-huan Tran, Jacques Louis, Sandrine Zanna, David Portehault, Andrea Zitolo, Michael Walls, Deizi Vanessa Peron, Moritz Schreiber, et al.

▶ **To cite this version:**

Hong Phong Duong, Jose Guillermo Rivera de la Cruz, Ngoc-huan Tran, Jacques Louis, Sandrine Zanna, et al.. Silver and Copper Nitride Cooperate for CO Electroreduction to Propanol. Angewandte Chemie International Edition, 2023, 10.1002/anie.202310788 . hal-04269621

HAL Id: hal-04269621
https://hal.science/hal-04269621

Submitted on 7 Nov 2023

HAL is a multi-disciplinary open access archive for the deposit and dissemination of scientific research documents, whether they are published or not. The documents may come from teaching and research institutions in France or abroad, or from public or private research centers.

L'archive ouverte pluridisciplinaire **HAL**, est destinée au dépôt et à la diffusion de documents scientifiques de niveau recherche, publiés ou non, émanant des établissements d'enseignement et de recherche français ou étrangers, des laboratoires publics ou privés.

Check for updates

A Journal of the Gesellschaft Deutscher Chemiker

Angewandte International Edition GDCh Chemie

www.angewandte.org

Accepted Article

Title: Silver and Copper Nitride Cooperate for CO Electroreduction to Propanol

Authors: Hong Phong Duong, Jose Guillermo Rivera de la Cruz, Ngoc-Huan Tran, Jacques Louis, Sandrine Zanna, David Portehault, Andrea Zitolo, Michael Walls, Deizi Vanessa Peron, Moritz W. Schreiber, Nicolas Menguy, and Marc Fontecave

This manuscript has been accepted after peer review and appears as an Accepted Article online prior to editing, proofing, and formal publication of the final Version of Record (VoR). The VoR will be published online in Early View as soon as possible and may be different to this Accepted Article as a result of editing. Readers should obtain the VoR from the journal website shown below when it is published to ensure accuracy of information. The authors are responsible for the content of this Accepted Article.

To be cited as: *Angew. Chem. Int. Ed.* **2023**, e202310788

Link to VoR: https://doi.org/10.1002/anie.202310788

WILEY VCH

10.1002/anie.202310788

15213773, ja, Downloaded from https://onlinelibrary.wiley.com/doi/10.1002/anie.202310788 by Sorbonne Université, Wiley Online Library on [16/10/2023]. See the Terms and Conditions (https://onlinelibrary.wiley.com/terms-and-conditions) on Wiley Online Library for rules of use; OA articles are governed by the applicable Creative Commons License

Accepted Manuscript

Silver and Copper Nitride Cooperate for CO Electroreduction to Propanol

Hong Phong Duong,[a] Jose Guillermo Rivera de la Cruz,[a] Ngoc-Huan Tran,[a*] Jacques Louis,[b] Sandrine Zanna,[c] David Portehault,[d] Andrea Zitolo,[e] Michael Walls,[f] Deizi Vanessa Peron,[g] Moritz W. Schreiber,[g] Nicolas Menguy,[h] Marc Fontecave[a*]

[a] Laboratoire de Chimie des Processus Biologiques, CNRS UMR 8229, Collège de France, Sorbonne Université, 11 Place Marcelin Berthelot, 75231 Paris Cedex 05, France

[b] Laboratoire de Chimie du Solide et Energie, CNRS UMR 8260, Collège de France, Sorbonne Université, 11 Place Marcelin Berthelot, 75231 Paris Cedex 05, France.

[c] Chimie ParisTech, PSL Research University, CNRS, Institut de Recherche de Chimie Paris (IRCP), 11 rue Pierre et Marie Curie, 75005 Paris, France

[d] Sorbonne Université, CNRS, Laboratoire de Chimie de la Matière Condensée de Paris (CMCP), 4 place Jussieu, Paris, France

[e] Synchrotron SOLEIL, L'Orme des Merisiers Saint-Aubin BP 48, 91192 Gif-sur-Yvette, France

[f] CNRS UMR 8502, Université Paris-Saclay, Laboratoire de Physique des Solides, F-91405 Orsay, France

[g] Total Research and Technology, Refining and Chemicals, Division CO_2 Conversion, Feluy, 7181 Seneffe, Belgium

[h] Sorbonne Université, UMR CNRS 7590, Institut de Minéralogie, de Physique des Matériaux et de Cosmochimie, 75005 Paris, France

*To whom correspondence may be addressed: ngoc-huan.tran@college-de-france.fr or marc.fontecave@college-de-france.fr

ABSTRACT

This article is protected by copyright. All rights reserved.

10.1002/anie.202310788

15213773, ja, Downloaded from https://onlinelibrary.wiley.com/doi/10.1002/anie.202310788 by Sorbonne Universite, Wiley Online Library on [16/10/2023]. See the Terms and Conditions (https://onlinelibrary.wiley.com/terms-and-conditions) on Wiley Online Library for rules of use; OA articles are governed by the applicable Creative Commons License

Accepted Manuscript

The need of carbon sources for the chemical industry, alternative to fossil sources, has pointed to CO_2 as a possible feedstock. While CO_2 electroreduction (CO_2R) allows production of interesting organic compounds, it suffers from large carbon losses, mainly due to carbonate formation. This is why, quite recently, tandem CO_2R, a two-step process, with first CO_2R to CO using a solid oxide electrolysis cell followed by CO electroreduction (COR), has been considered, since no carbon is lost as carbonate in either step. Here we report a novel copper-based catalyst, silver-doped copper nitride, with record selectivity for formation of propanol (Faradic efficiency: 45%), an industrially relevant compound, from CO electroreduction in gas-fed flow cells. Selective propanol formation occurs at metallic copper atoms derived from copper nitride and is promoted by silver doping as shown experimentally and computationally. In addition, the selectivity for C_{2+} liquid products (Faradic efficiency: 80%) is among the highest reported so far. These findings open new perspectives regarding the design of catalysts for production of C_3 compounds from CO_2.

Introduction

Electroreduction of CO_2 allows storing intermittent solar and wind energies as well as producing important energy-dense organic molecules (hydrocarbons, alcohols, olefins) for the chemical industry.[1] In spite of tremendous efforts and progresses, linked to the development of efficient catalysts, notably copper-based ones since Cu is the only metal allowing significant C-C coupling reactions, and electrolyzers, notably gas-fed flow cells and membrane electrode assemblies, however, CO_2 electroreduction faces a number of problems which require further optimization, before it can be upscaled towards industrial implementation.[1a, 2] One of the most relevant issues is the formation of carbonate resulting from the reaction of CO_2 with hydroxide, an inevitable product of CO_2 reduction.[3] Formation of carbonate has several detrimental impacts: acidification of the electrolyte, increased interfacial resistance, precipitation of carbonate on the gas diffusion cathode eventually causing flooding. This makes catholyte recycling an energy-intense and expensive process. Furthermore, carbonate is prone to crossover through the membrane leading to its accumulation in the anode compartment where it is hydrolyzed to CO_2, thus implying extra costs associated with recuperation of CO_2 from the O_2 stream.[3b] There are two possible solutions addressing this issue. The first one consists in acidic CO_2 electrolysis which very recently proved practical, as appropriate engineering allows

This article is protected by copyright. All rights reserved.

15213773, ja, Downloaded from https://onlinelibrary.wiley.com/doi/10.1002/anie.202310788 by Sorbonne Universite, Wiley Online Library on [16/10/2023]. See the Terms and Conditions (https://onlinelibrary.wiley.com/terms-and-conditions) on Wiley Online Library for rules of use; OA articles are governed by the applicable Creative Commons License

Accepted Manuscript

high Faradaic efficiency for CO_2 reduction (CO_2R) with only little H_2 evolution, even in such acidic conditions.[4] The second one is based on so-called tandem CO_2R, a two-step process, with first CO_2R to CO using a solid oxide electrolysis cell (SOEC) followed by CO electroreduction (COR), since no carbon is lost as carbonate in either step.[5] This attractive scenario has recently led to an increasing number of studies aiming at developing selective, stable and cheap Cu-based catalysts for electrochemical conversion of CO into C_{2+} products, ethylene, alcohols and acetic acid.[6] However, still few variations have been studied as far as catalysts are concerned and most investigations have focused on polycrystalline Cu, commercial Cu nanoparticles and oxide-derived Cu catalysts which proved efficient in promoting C-C coupling reactions. On our side, we recently reported an original dendritic and porous Cu material which proved highly selective for ethylene production from COR.[6a, 6b]

Here we report our efforts to convert CO selectively into n-propanol, a high-energy liquid compound, using electricity as an energy source. Propanol is currently produced from reaction of CO with fossil-derived ethylene in a process requiring hydrogen and high temperature and pressure and it is tempting to evaluate whether direct electroreduction of CO could be an alternative. There is a high interest in the industry for new, fossil-free, methods for producing propanol, as there are a lot of important C3 commodity chemicals.[7] Until very recently, electrolysis of CO using Cu-based catalysts showed very little selectivity towards propanol. However, two very recent studies have shown that metal-doped Cu materials promote CO adsorption, stabilize C_2 intermediates and thus facilitate C-C and C-C_2 coupling, thus improving C3 product formation.[6c, 6d] In particular, commercial Cu nanoparticles doped with Ag led to a high n-propanol FE of 25-30%, higher than that of pristine Cu (20%), which could be further increased to 36% by adding Ru as an additional dopant.[6c, 6d] To our knowledge these numbers were the highest reported ones for CO electroreduction to n-propanol.

We discovered and report now that Ag-doped copper nitride is a highly selective electrocatalyst for COR to n-propanol leading to a record FE value of 45% at industrially-relevant current densities of 150 mA cm^{-2}, in an alkaline flow electrolyser. The alkaline catholyte (KOH) indeed ensures relatively stable local pH on the electrode surface, optimizes conductivity and promotes C-C coupling, notably towards production of C_{2+} oxygenates.[2b, 6f] Interestingly, we observed that the selectivity, in terms of liquid products (ethanol, propanol, acetate) formation, could be finely controlled via modification of the electrolyte KOH concentration.

This article is protected by copyright. All rights reserved.

15213773, ja, Downloaded from https://onlinelibrary.wiley.com/doi/10.1002/anie.202310788 by Sorbonne Universite, Wiley Online Library on [16/10/2023]. See the Terms and Conditions (https://onlinelibrary.wiley.com/terms-and-conditions) on Wiley Online Library for rules of use; OA articles are governed by the applicable Creative Commons License

Accepted Manuscript

Results

In the following the studied materials are symbolized as $CuM_{x\%}N_{th}$, with x giving the mol% value of the doping metal M, as in the galvanic reaction solution, t the time in hours used for the nitridation step, and N to indicate the presence of nitride in the material. Preparation of $CuM_{x\%}N_{th}$ is described in detail in the Supporting Information (SI) section and summarized in Figure S1.[8] Briefly, doping copper nanoparticles (CuNPs) with M (Ag, Pd, Au) was carried out via a galvanic replacement reaction using a solution of $AgNO_3$, $PdCl_2$ and $HAuCl_4$, respectively. The obtained bi-metallic $CuM_{x\%}$ materials were then submitted to calcination at 500 °C in air during 1h and then pyrolyzed in the presence of $NaNH_2$ at 170 °C. The nitridation reaction time varied between 10 and 60 hours. For example, a sample obtained with 5 % of Ag in the galvanic exchange reaction solution and after nitridation during 20 h was named as $CuAg_{5\%}N_{20h}$. Control samples $CuM_{x\%}$, for which the nitridation step was omitted, and CuN_{th}, for which the galvanic exchange step was omitted, were also prepared. For electrochemical experiments, 1.2 mg of each sample, mixed with Nafion, was deposited on a Gas Diffusion Layer (GDL) to generate a Gas Diffusion Electrode (GDE).

Figure 1a shows the Scanning Electron Microscopy (SEM) images of $CuAg_{5\%}$ and $CuAg_{5\%}N_{20h}$ while those of CuNPs and CuN_{20h} are displayed in Figure S2. They indicate that the calcination/nitridation treatment results in a significant change of the morphology of the material. As compared to CuNPs and $CuAg_{5\%}$, containing homogeneous particles of 50-60 nm in size (as determined by SEM), the samples obtained after nitridation are more heterogeneous, with much smaller nanoparticles (down to 5 nm) together with nanorods. They also display slightly larger porosity and roughness, reflecting greater nanostructuration (Figure 1a, Figure S2). In contrast, the galvanic replacement reaction had little effect on the morphology of Cu NPs (Figure S2).

Powder X-ray diffraction (XRD) patterns show that $CuAg_{5\%}N_{20h}$ contained metallic Cu, Cu_3N and Ag and no CuO could be detected, confirming the efficiency of the nitridation step (Figure 1b). Cu_3N was present in CuN_{20h} but not in $CuAg_{5\%}$ as expected. XRD patterns of $CuAg_{x\%}N_{20h}$ samples with x= 2, 5 and 8% Ag indicated the presence of the three components, however, as expected, with different Ag signal intensities (Figure S3). Metallic Cu was present in very low amounts (for example about 3% in the $CuAg_{5\%}N_{20h}$ sample as determined in Figure S3b). Similarly, the presence of other metal dopants in $CuM_{5\%}N_{20h}$ (M= Au and Pd) was

This article is protected by copyright. All rights reserved.

10.1002/anie.202310788

confirmed by XRD (Figure S4). XRD analysis of $CuAg_{5\%}N_{th}$ samples with t varying from 10 to 60 h showed that characteristic Cu_3N signals appeared soon at 10 h and increased up to 20 h, became less intense after more prolonged reaction (> 25 h) and disappeared at 60h (Figure S5). X ray photoelectron spectroscopy (XPS) analysis further confirmed the composition of the $CuAg_{5\%}N_{20h}$ material.

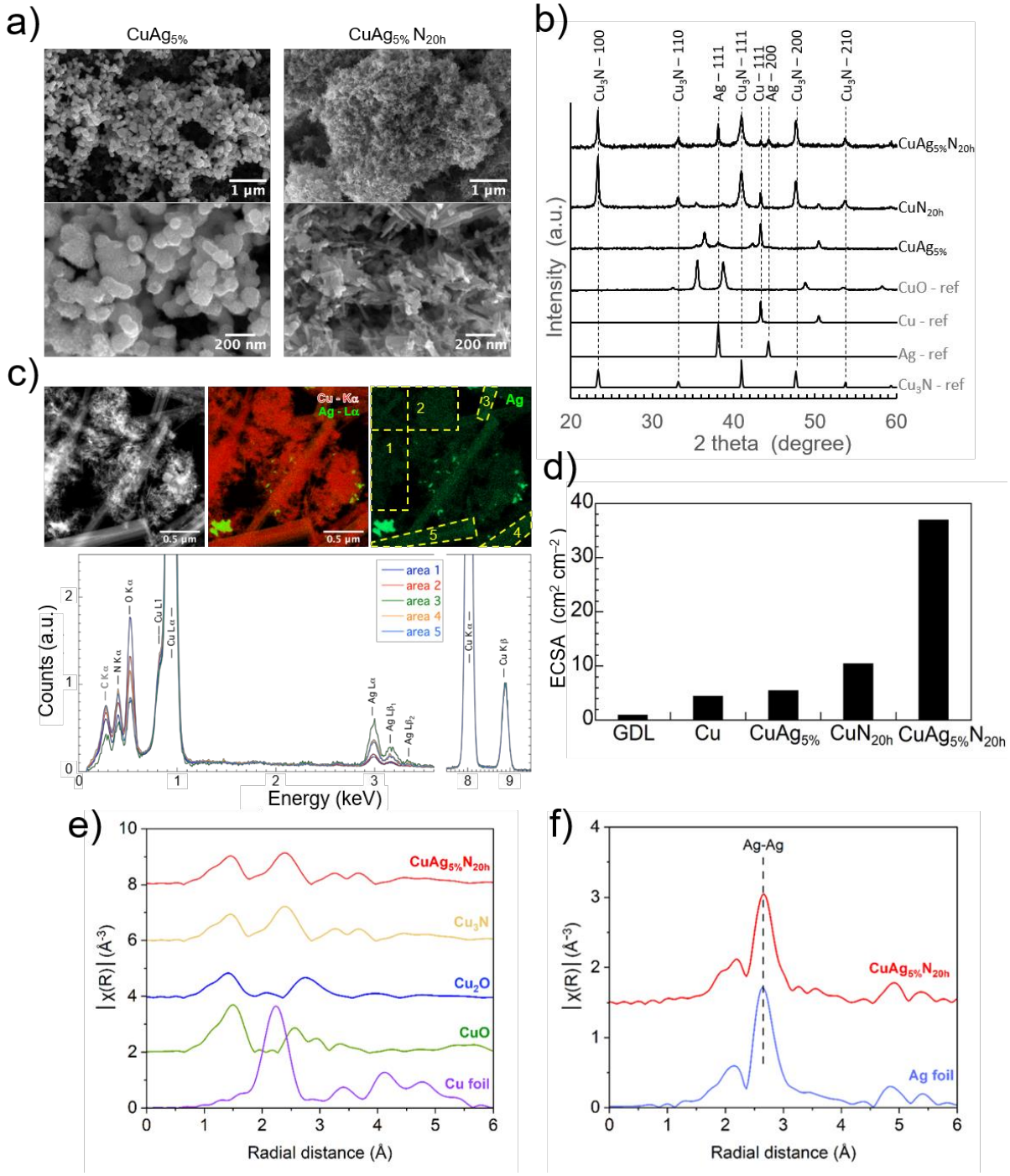

Figure 1. a) SEM images at different magnifications of $CuAg_{5\%}$ and $CuAg_{5\%}N_{20h}$; b) XRD characterization of different samples and the reference materials; c) STEM analysis of

This article is protected by copyright. All rights reserved.

15213773, ja, Downloaded from https://onlinelibrary.wiley.com/doi/10.1002/anie.202310788 by Sorbonne Universite, Wiley Online Library on [16/10/2023]. See the Terms and Conditions (https://onlinelibrary.wiley.com/terms-and-conditions) on Wiley Online Library for rules of use; OA articles are governed by the applicable Creative Commons License

Accepted Manuscript

15213773, ja, Downloaded from https://onlinelibrary.wiley.com/doi/10.1002/anie.202310788 by Sorbonne Universite, Wiley Online Library on [16/10/2023]. See the Terms and Conditions (https://onlinelibrary.wiley.com/terms-and-conditions) on Wiley Online Library for rules of use; OA articles are governed by the applicable Creative Commons License

Accepted Manuscript

$CuAg_{5\%}N_{20h}$. Top left: STEM-HAADF image (left); Top middle: STEM-XEDS composite (Cu-Kα and Ag-Lα) elemental map; Top right: STEM-XEDS Ag-Lα elemental map, Ag nanocrystals appear as bright green spots; Bottom: XEDS spectra related to the labelled areas (1 – 5) in Top right image; the intensity of these spectra has been normalized to the Cu-Kα line. d) ECSA of different materials deposited on the GDE; e) Cu K-edge and f) Ag K-edge EXAFS spectra of $CuAg_{5\%}N_{20h}$ and the references.

In agreement with XRD results, Transmission Electron Microscopy (TEM) analyses performed on $CuAg_{5\%}N_{20h}$ confirmed the presence of Cu_3N, metallic Ag and metallic Cu (Figure S7). TEM observations revealed a broad size distribution of Cu_3N nanoparticles and rods from tens nm to few microns (Figure 1c and S7a). Furthermore, STEM–HAADF and HRTEM showed that Cu_3N rods exhibited a finely grained and porous structure, resulting from an oriented aggregation of small elongated crystals (Figure S7a, S7b and S7d). Moreover, from scanning TEM coupled with X-ray energy dispersive spectroscopy (STEM-XEDS) or electron energy loss spectroscopy (STEM-EELS), it appeared that Ag is present in two forms: (*i*) metallic Ag particles with a size of between 10 nm and 1 µm (figure S7c and d) and (*ii*) homogeneously dispersed among Cu_3N crystals in variable proportions (estimated to 1 – 3 at. %) in agreement with XPS measurements. The absence of Ag nanoclusters (i.e. smaller than 1 nm) at the surface of Cu_3N particles has been deduced from HR-STEM and STEM-EELS analyses (Figure S7a and e), suggesting a substitutional doping of Ag atoms at the surface of Cu_3N nanocrystals.

Cu K-edge EXAFS analysis showed that Cu is mainly present as Cu_3N (Figure 1e). Metallic Cu is too scarce to be detectable in the EXAFS spectrum. The presence of small Ag particles was confirmed via Ag K-edge EXAFS analysis showing a spectrum similar to that of metallic Ag foil (Figure 1f).

Electrochemical surface areas (ECSAs) of the different samples were determined after deposition on the GDL via measurement of double layer capacitances (CDLs) of the resulting electrodes (Figure 1d and Figure S8). A larger ECSA value of about 37 $cm^2\ cm^{-2}$ was obtained for $CuAg_{5\%}N_{20h}$ in agreement with the observed increased roughness revealed by TEM and STEM observations (Figure 1 and Figure S7). Consistently, the specific area, obtained by the Brunauer-Emmett-Teller (BET) method, also increased significantly after Ag-doping and nitridation (Table S1).

This article is protected by copyright. All rights reserved.

10.1002/anie.202310788

Electroreduction of CO was carried out using a gas-fed flow electrolyzer. CO was fed on the back side of the GDE and the reaction took place at a triple-phase CO gas/solid catalyst surface/liquid electrolyte interface (Figure 2a). A circulating 1.0 M KOH electrolyte was used for both anodic and cathodic compartments, and they are separated by a sustainion anion exchange membrane (SAEM). During electrolysis, a gas chromatography online system, connected to the gas outlet of the flow cell allowed quantification of gas products. As shown below, only ethylene, with no trace of methane and ethane, and small amounts of H_2 could be observed. The liquid phase was analyzed by NMR spectroscopy and shown to contain the following liquid products: ethanol, acetate and n-propanol.

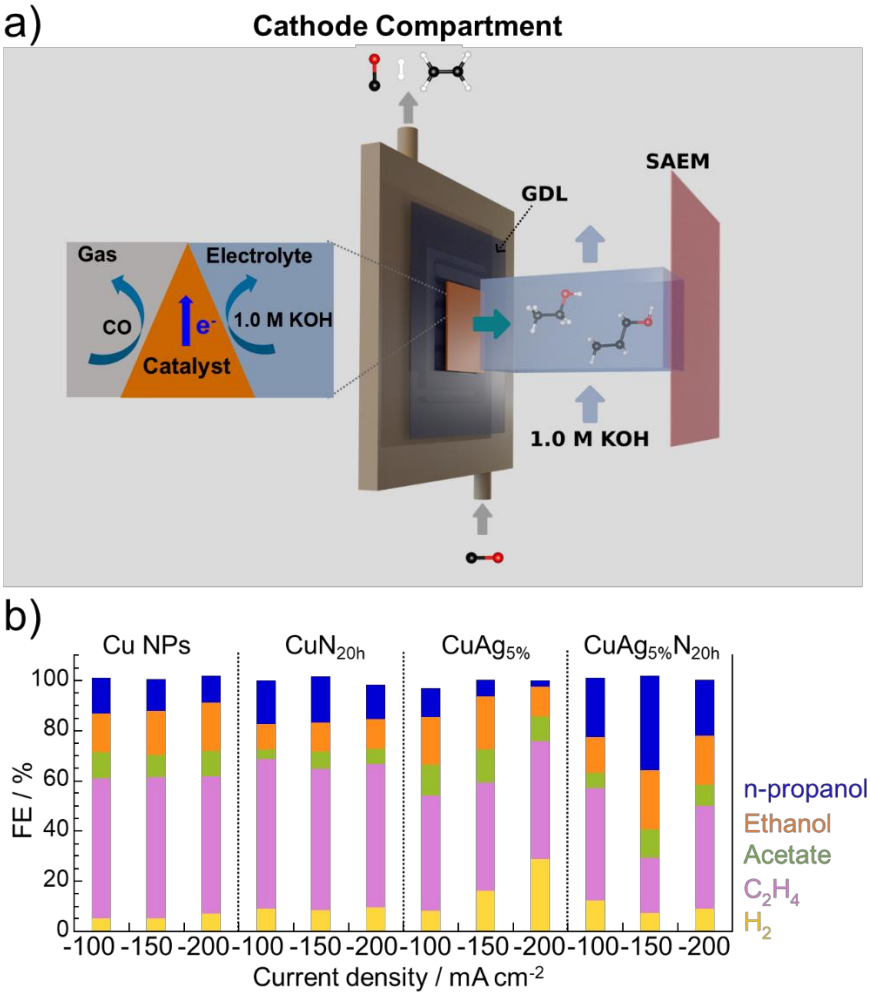

Figure 2. a) scheme of cathode compartment in flow electrolyzer for CO electroreduction and b) product distribution after CO electroreduction for 30 minutes in 1.0 M KOH electrolyte using different catalysts: Cu NPs, CuN_{20h}, $CuAg_{5\%}$ And $CuAg_{5\%}N_{20h}$. Conditions: anode (Ni foam); anolyte and catholyte (KOH 1 M); applied current density (100-200 mA cm^{-2} for 0.5 h); CO

This article is protected by copyright. All rights reserved.

15213773, ja, Downloaded from https://onlinelibrary.wiley.com/doi/10.1002/anie.202310788 by Sorbonne Universite, Wiley Online Library on [16/10/2023]. See the Terms and Conditions (https://onlinelibrary.wiley.com/terms-and-conditions) on Wiley Online Library for rules of use; OA articles are governed by the applicable Creative Commons License

Accepted Manuscript

15213773, ja, Downloaded from https://onlinelibrary.wiley.com/doi/10.1002/anie.202310788 by Sorbonne Universite, Wiley Online Library on [16/10/2023]. See the Terms and Conditions (https://onlinelibrary.wiley.com/terms-and-conditions) on Wiley Online Library for rules of use; OA articles are governed by the applicable Creative Commons License

Accepted Manuscript

flow (10 ml.min^{-1}). The results are an average of three independent experiments. SAEM: Sustainion anion exchange membrane.

CO electroreduction took place at relatively moderate cathode potentials as shown by Linear Sweep Voltammetry (LSV) using $CuAg_{5\%}N_{20h}$ as the catalyst (Figure S9). During the first scan, a reduction peak was observed at about 0 V vs RHE which was assigned to the reduction of Cu^+ (in Cu_3N) into metallic Cu^0 and catalytic CO reduction was observed at more cathodic potentials. The reduction peak at 0 V vs RHE became almost invisible during the next scans suggesting full reduction of Cu_3N into metallic Cu^0. The absence of the Cu_3N component in the material after 3 consecutive scans was confirmed by XRD (Figure S10). The presence of Cu_2O is due to surface re-oxidation during exposure to air as shown below from *in situ* XRD experiments. This suggests that the actual catalyst for CO electroreduction was Ag-doped nitride-derived Cu^0. LSVs (3rd scan) of control samples during CO electroreduction are displayed in Figure S11a, showing that the highest catalytic activity, in terms of current density for a given cathodic potential, was obtained with $CuAg_{5\%}N_{20h}$. In this case, the catalytic wave allowed reaching current densities of – 100 and – 200 mA cm^{-2} with a cathodic potential spanning a broad range of values, from – 0.5 to -1.1 V vs RHE, respectively (Figure S11a). This was confirmed by electrolysis of CO using $CuAg_{5\%}N_{20h}$ at different current densities giving stable cathodic potentials during 30 minutes (Figure S11b).

The results of bulk CO electrolysis at different controlled applied current densities (100, 150 and 200 mA cm^{-2}) for 30 minutes using $CuAg_{5\%}N_{20h}$ and control samples, CuNPs, CuN_{20h} and $CuAg_{5\%}$, are presented in Figure 2b. All the catalysts exhibited very good selectivity for CO reduction with very low Faradic Efficiency for H_2 production (FE_{H_2}) in most experiments. Among these samples, $CuAg_{5\%}N_{20h}$ showed remarkable selectivity for C_{2+} alcohols (ethanol + n-propanol). At -150 mA cm^{-2}, n-propanol was formed with a high $FE_{C_3H_8O}$ of 39%, together with significant amounts of ethanol ($FE_{C_2H_6O}$ = 23%) and acetate ($FE_{C_2H_4O_2}$ =11%), so that the total FE for liquid products was about 73%. As FE_{H_2} was only 7 % and $FE_{C_2H_4}$ (for ethylene) was 19 % the total FE for C_{2+} product was about 92%. In contrast, at the same applied current density, all the other studied materials produced ethylene as the major reaction product with $FE_{C_2H_4}$ ranging from 42 % ($CuAg_{5\%}$) to 57% (CuNPs). At all current densities, $CuAg_{5\%}N_{20h}$ displayed the largest selectivity towards n-propanol production (Figure 2b and Figure S12). Comparison with control samples indicates that the presence of both Cu_3N and Ag in the precursor material was critical in promoting n-propanol formation (Figure 2b).

This article is protected by copyright. All rights reserved.

10.1002/anie.202310788

Considering that oxide-derived copper was previously reported as an excellent catalyst for CO electroreduction to ethanol,[6g] we have prepared CuO and $CuOAg_{5\%}$, via calcination of CuNPs and $CuAg_{5\%}$, respectively, in air at 500 °C during 1h. These materials indeed displayed relatively higher selectivity for ethanol but much lower ability to generate n-propanol (Figure S13a). This reveals significantly different reactivity of nitride-derived Cu active sites as compared to oxide-derived ones.

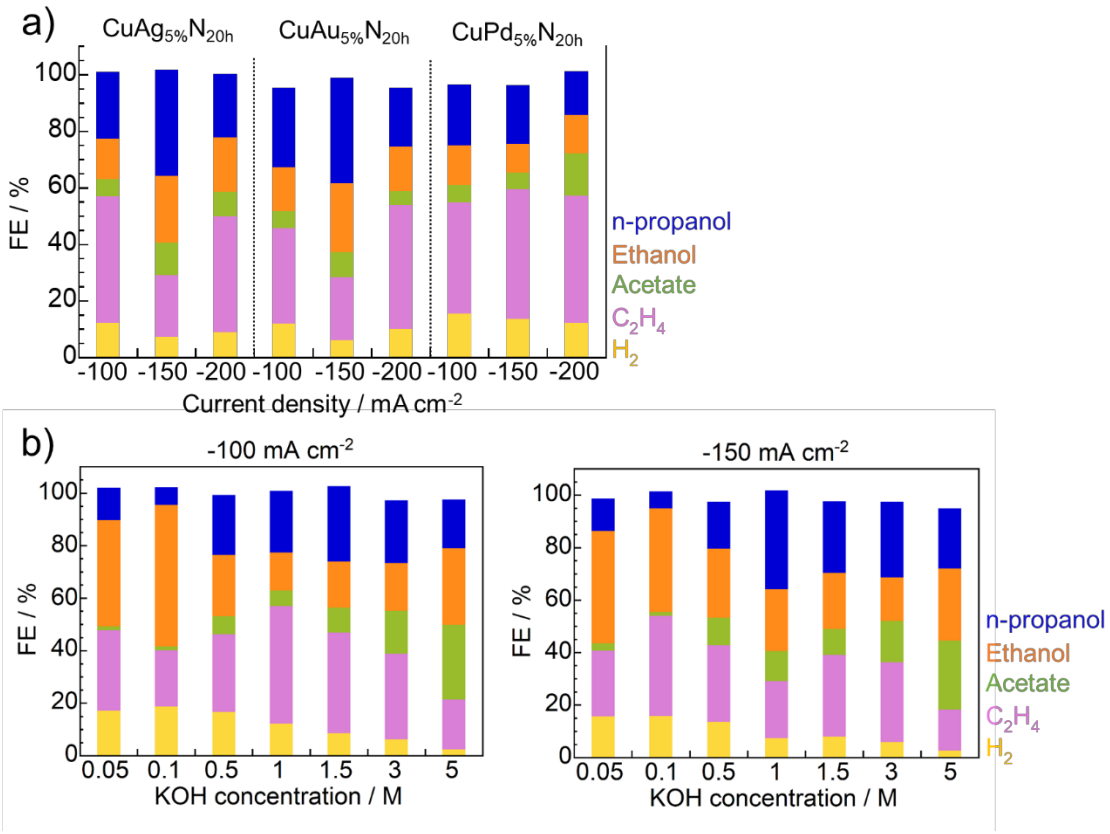

Figure 3. Product distribution during CO electroreduction in 1.0 M KOH: a) using $CuM_{5\%}N_{20h}$ catalysts (with M = Ag, Au, Pd; b) using $CuAg_{5\%}N_{20h}$ at different KOH concentration at the cathodic current density of -100 and -150 mA cm^{-2}. Conditions: anode (Ni foam), anolyte and catholyte (KOH 1.0 M), applied current (100-200 mA cm^{-2} for 0.5 h), CO flow (10 mL min^{-1}).

A similar capacity to catalyze CO conversion into C_{2+} alcohols, with n-propanol as the major product, was observed with the $CuAu_{5\%}N_{20h}$ sample, which displayed a high FE for propanol of 37% at -150 mA cm^{-2}, and low $FE_{C_2H_4}$ and FE_{H2} values (Figure 3a). In contrast $CuPd_{5\%}N_{20h}$ was more selective for ethylene and led to slightly higher yields of H_2 production.

This article is protected by copyright. All rights reserved.

15213773, ja, Downloaded from https://onlinelibrary.wiley.com/doi/10.1002/anie.202310788 by Sorbonne Universite, Wiley Online Library on [16/10/2023]. See the Terms and Conditions (https://onlinelibrary.wiley.com/terms-and-conditions) on Wiley Online Library for rules of use; OA articles are governed by the applicable Creative Commons License

Accepted Manuscript

15213773, ja, Downloaded from https://onlinelibrary.wiley.com/doi/10.1002/anie.202310788 by Sorbonne Universite, Wiley Online Library on [16/10/2023]. See the Terms and Conditions (https://onlinelibrary.wiley.com/terms-and-conditions) on Wiley Online Library for rules of use; OA articles are governed by the applicable Creative Commons License

Accepted Manuscript

Doping with Ru greatly degraded the selectivity for CO reduction, as $CuRu_{5\%}N_{20h}$ promoted H_2 formation (FE_{H2} > 40 %) and gave little propanol (Figure S13b). In the following, only the Ag-doped material is studied.

Considering that Ag is also present in the form of few nanoparticles (NPs) we studied their activity using GDEs containing AgNPs alone or mixed with CuN_{20h}, with 5% Ag. The results clearly showed that AgNPs cannot have any catalytic role in propanol formation even in mixture with copper nitride (Figure S14).

The $CuAg_{5\%}N_{20h}$ material was characterized by electron microscopy after 1h CO electrolysis at -150 mA cm^{-2} in 1M KOH. The SEM image showed that the material was still a mixture of nanoparticles and nanorods. The main difference with the initial material resided in the increased roughness of the surface of the nanorods (Figure S15). Further characterizations were carried out by STEM and SAED analysis (Figure S16) confirming that Cu_3N was no longer present in the material after electrolysis, and only Cu_2O, Cu^0 and Ag^0 were observed, as confirmed by post-electrolysis XRD analysis (Figure S17). As shown below, the presence of Cu_2O is likely derived from *ex-situ* manipulation of the samples in air. In addition, elemental mapping analysis also demonstrated that the homogeneous distribution of Ag in the bulk material was retained. It has also to be noticed that nanoparticles exhibited a significant porosity at the nanometric scale (Figure S15). XPS analysis confirmed the presence of Ag and the absence of N (Figure S18). ECSA after electrolysis of $CuAg_{5\%}N_{20h}$ was still high, at about 30 cm^2 cm^{-2} (Figure S19).

An extensive series of experiments using $CuAg_{x\%}N_{th}$ as the catalyst were carried out in order to investigate the effect of different parameters on the catalytic performances for CO electroreduction: (i) the reaction time during the nitridation step (varying the t parameter); (ii) the amount of Ag (varying the x parameter); (iii) the CO flow rate; (iv) the amount of catalyst deposited on the GDE; (v) KOH concentration.

First, the highest yields of propanol ($FE_{C_3H_8O}$ > 20%) were obtained for $CuAg_{5\%}N_{th}$ materials obtained with short nitridation reaction times (t from 10 to 20 h), while they greatly decreased for t > 25 h (Figure S20). This is quite consistent with the observation, derived from XRD characterization, that the highest contents of Cu_3N were obtained with low nitridation times (Figure S5) thus confirming the importance of the presence of Cu_3N in the initial material.

Second, the selectivity of the catalyst can be tuned by varying the amount of Ag (Figure S21). However, the optimal Ag amount depends on the applied current, with no clear trend: the

This article is protected by copyright. All rights reserved.

15213773, ja, Downloaded from https://onlinelibrary.wiley.com/doi/10.1002/anie.202310788 by Sorbonne Universite, Wiley Online Library on [16/10/2023]. See the Terms and Conditions (https://onlinelibrary.wiley.com/terms-and-conditions) on Wiley Online Library for rules of use; OA articles are governed by the applicable Creative Commons License

Accepted Manuscript

highest FE values for n-propanol were obtained with $CuAg_{2\%}N_{20h}$ at -100 mA cm^{-2} (35 %) and with $CuAg_{5\%}N_{20h}$ at -150 mA cm^{-2} (39 %).

Third, Figure S22 shows the results of controlled current CO electrolysis in 1.0 M KOH at -150 mA cm^{-2} at different CO flow rates. Significant variations could be observed. In particular FE for n-propanol production increased as a function of the CO flow rate, was maximum at an intermediate value of 10 mL min^{-1} and then decreased upon further increase of the flow rate. It is likely that increasing CO coverage allows reaching an optimal ratio of adsorbed CO and C_2 intermediates for n-propanol synthesis while, above that limit, CO prevents these key C_2 intermediates from binding to the active sites on the surface, as recently raised by MTM Koper and collaborators.[9]

Fourth, Figure S23 shows that the highest selectivity for n-propanol production was obtained with 1.2 mg catalyst deposited on 1 cm^2 GDE.

Fifth, CO electroreduction catalyzed by $CuAg_{5\%}N_{20h}$ was carried out at different current densities (-100, -150 and -200 mA cm^{-2}) using electrolytes containing different KOH concentrations ([KOH]) (from 0.05 M to 5.0 M). As shown from LSVs the larger [KOH] the higher the catalytic current correlating with increased conductivity (Figure S24a). The product distributions, in terms of FEs, are presented in Figure 3b and Figure S24b. As expected, from similar observations in previous studies,[10] H_2 production decreased and acetate formation increased with increased [KOH], up to 29% at 5.0 M KOH. As $FE_{C_2H_4}$ and FE_{H_2} were the lowest at the highest [KOH], the total FE for liquid products at 5.0 M KOH was at about 80 %. As for n-propanol, one clearly observed an increase of $FE_{C_3H_8O}$ as [KOH] increased up to 1.0 M ($FE_{C_3H_8O}$ = 39% at -150 mA cm^{-2}), followed by a decrease upon further increase of [KOH]. Finally, remarkable selectivity for ethanol was obtained at low [KOH], with a maximal $FE_{C_2H_6O}$ of 55 %, at 0.1 M KOH and at -100 mA cm^{-2} together with very little formation of acetate and n-propanol. The highest FE for C_{2+} alcohol production (62%) was obtained at -150 mA cm^{-2} in 1.0 M KOH. The experiment shown in Figure S24c gives some insight into the role of pH and K^+ concentration in tuning the selectivity. Starting with 0.1 M KOH, providing large yields of ethanol, addition of K^+ in the form 0.9 M KCl led to a decrease of $FE_{C_2H_6O}$ and a large increase of $FE_{C_3H_8O}$, reflecting the specific role of K^+ in promoting propanol formation. On the other hand, further increase of propanol formation and decrease of $FE_{C_2H_4}$ was obtained with 1 M KOH as the catholyte, showing the importance of alkalinity for increasing the propanol/ethylene ratio.

This article is protected by copyright. All rights reserved.

10.1002/anie.202310788

15213773, ja, Downloaded from https://onlinelibrary.wiley.com/doi/10.1002/anie.202310788 by Sorbonne Universite, Wiley Online Library on [16/10/2023]. See the Terms and Conditions (https://onlinelibrary.wiley.com/terms-and-conditions) on Wiley Online Library for rules of use; OA articles are governed by the applicable Creative Commons License

Accepted Manuscript

Interestingly, using 1.0 M CsOH as the catholyte resulted in a further increase of FE_{C3H8O} up to a remarkable value of 45%, a FE for C_{2+} alcohol production of 65% and a FE for liquid products of 80 % (Figure S24 and S25).This is in line with previous reports showing that such cations, with the smallest hydrated radius, allowing higher concentration at the cathode surface, can generate a stronger double layer field which contributes to enhance the adsorption of CO and the stabilization of intermediates towards multicarbon products.[11]

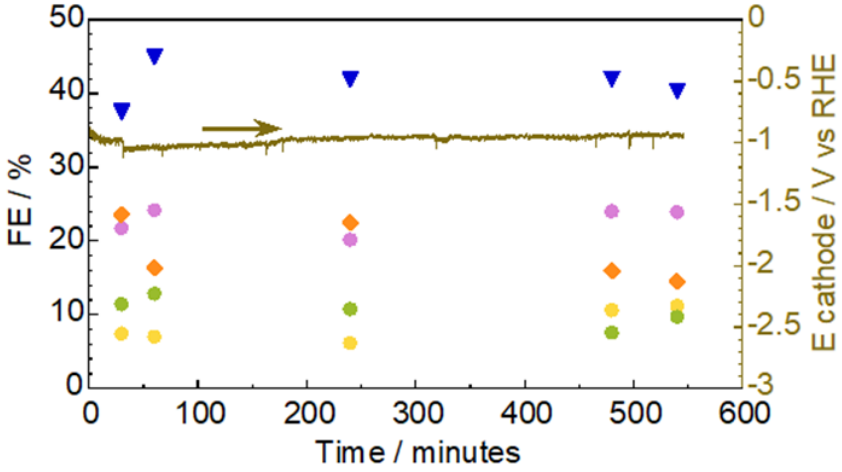

Figure 4. Long term electrolysis. CO electroreduction catalyzed by $CuAg_{5\%}N_{20h}$ or at -150 mA cm^{-2} in 1.0 M KOH solution. The cathodic potential is monitored during electrolysis with the product distribution during electrolysis. The product distribution is presented as FE for n-propanol (blue triangle), ethanol (orange square), acetate (green circle), ethylene (magenta circle) and H_2 (yellow circle).

A long-term (9 hours) electrolysis at -150 mA cm^{-2} using $CuAg_{5\%}N_{20h}$ in 1.0 M KOH has been carried out (Figure 4). The system proved stable during the 9 hours, with a constant cathodic potential at -1.0 V, a stable $FE_{C_3H_8O}$ at 42 +/- 3 % and with only slight variations of the FE values for the other products. For safety reasons, electrolysis could not be run longer. In addition, a long-term electrolysis at -100 mA cm^{-2} using 0.1 M KOH has shown a stable production of ethanol with $FE_{C_2H_6O}$ of about 56 % (Figure S27).

This article is protected by copyright. All rights reserved.

10.1002/anie.202310788

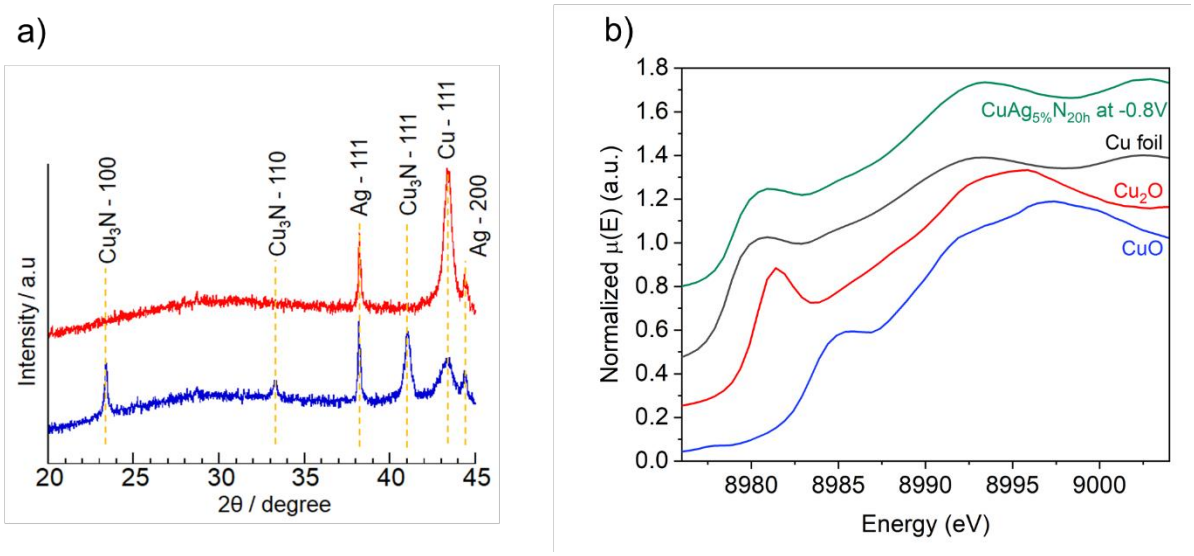

Figure 5. a) *in-situ* XRD patterns of $CuAg_{5\%}N_{20h}$ before (blue) and during (red) electrochemical CO reduction and b) *in-situ* Cu K-edge XANES spectra of $CuAg_{5\%}N_{20h}$ (green) during electrochemical CO reduction (-0.8 V vs RHE) and of reference samples.

To get some insights into the catalytic material in action, *in-situ* characterization has been carried out. Using a homemade electrochemical cell designed for *in-situ* XRD measurement (see experimental section), the XRD pattern of the $CuAg_{5\%}N_{20h}$ electrode, under an applied cathodic current density of -150 $mAcm^{-2}$ in a CO-saturated 1.0 M KOH solution as the catholyte, was obtained. One should note that the XRD pattern was recorded only up to 45 degree because of the strong signals of the Be window of the cell above that limit (Figure S28). Comparison of the diffractogram before electrolysis (Figure 5a, bottom) with that during electrolysis (Figure 5a, top) clearly demonstrated that, under catalytic conditions, Cu_3N was reduced to Cu° and no more observable so that only Cu° and Ag° were present in the material. It is important to note that no Cu_2O could be detected either, while it was observed when the reduced sample was exposed to air (see for example Figures S10 and S16). *In-situ* XANES analysis confirmed that upon application of a cathodic current density to the $CuAg_{5\%}N_{20h}$ electrode, the Cu K-edge was immediately shifted to low energies, which indicated a reduction from initial Cu^+ to Cu° (Figure 5b).

The energetics of the C_1-C_2 coupling reactions were studied by periodic DFT calculations (computational details in the Supplementary Information). We focused on two catalytic systems: pure Cu, represented as a Cu(100) slab and Ag-doped Cu using a model in which an Ag atom has been substituted for one surface Cu atom replacing one surface Cu atom at a density corresponding to a 3% doping concentration, in agreement with experimental data

This article is protected by copyright. All rights reserved.

15213773, ja, Downloaded from https://onlinelibrary.wiley.com/doi/10.1002/anie.202310788 by Sorbonne Universite, Wiley Online Library on [16/10/2023]. See the Terms and Conditions (https://onlinelibrary.wiley.com/terms-and-conditions) on Wiley Online Library for rules of use; OA articles are governed by the applicable Creative Commons License

Accepted Manuscript

10.1002/anie.202310788

15213773, ja, Downloaded from https://onlinelibrary.wiley.com/doi/10.1002/anie.202310788 by Sorbonne Universite, Wiley Online Library on [16/10/2023]. See the Terms and Conditions (https://onlinelibrary.wiley.com/terms-and-conditions) on Wiley Online Library for rules of use; OA articles are governed by the applicable Creative Commons License

Accepted Manuscript

(Figure S29). Our modeling approach builds upon previous successful studies that have investigated Ag-doped catalysts prepared using the galvanic replacement reaction.[6c] Consistent with these previous findings,[12] our results indicate a highly asymmetric Ag-doped surface, with compressed bond distances and surface stress, as a consequence of the Ag atomic radius being larger than that of Cu (Figure S29). Wang et al. have found that this compressive stress can favor C_1-C_2 coupling reactions.[6c, 13] Furthermore, the interaction between Cu and Ag atoms is expected to induce modifications of the electronic structure of Cu. As a consequence, the combined effects of structural and electronic changes lead to the formation of surface asymmetric Cu atoms, which can significantly influence the interaction with the different adsorbates.

We have selected a collection of C_1-C_2 coupling steps along the most accepted path, on Cu(100), towards the formation of C_2 surface intermediates.[10, 14] This in line with the findings of Tang et al.,[15] identifying these reactions as the most feasible steps towards the formation of C_3 products on Cu(100). The reaction mechanism corresponding to the selected steps is shown on Figure S29a. Schematic representations of the geometries of initial, final and transition states can be found in Supplementary Information, section 4.5.

This article is protected by copyright. All rights reserved.

10.1002/anie.202310788

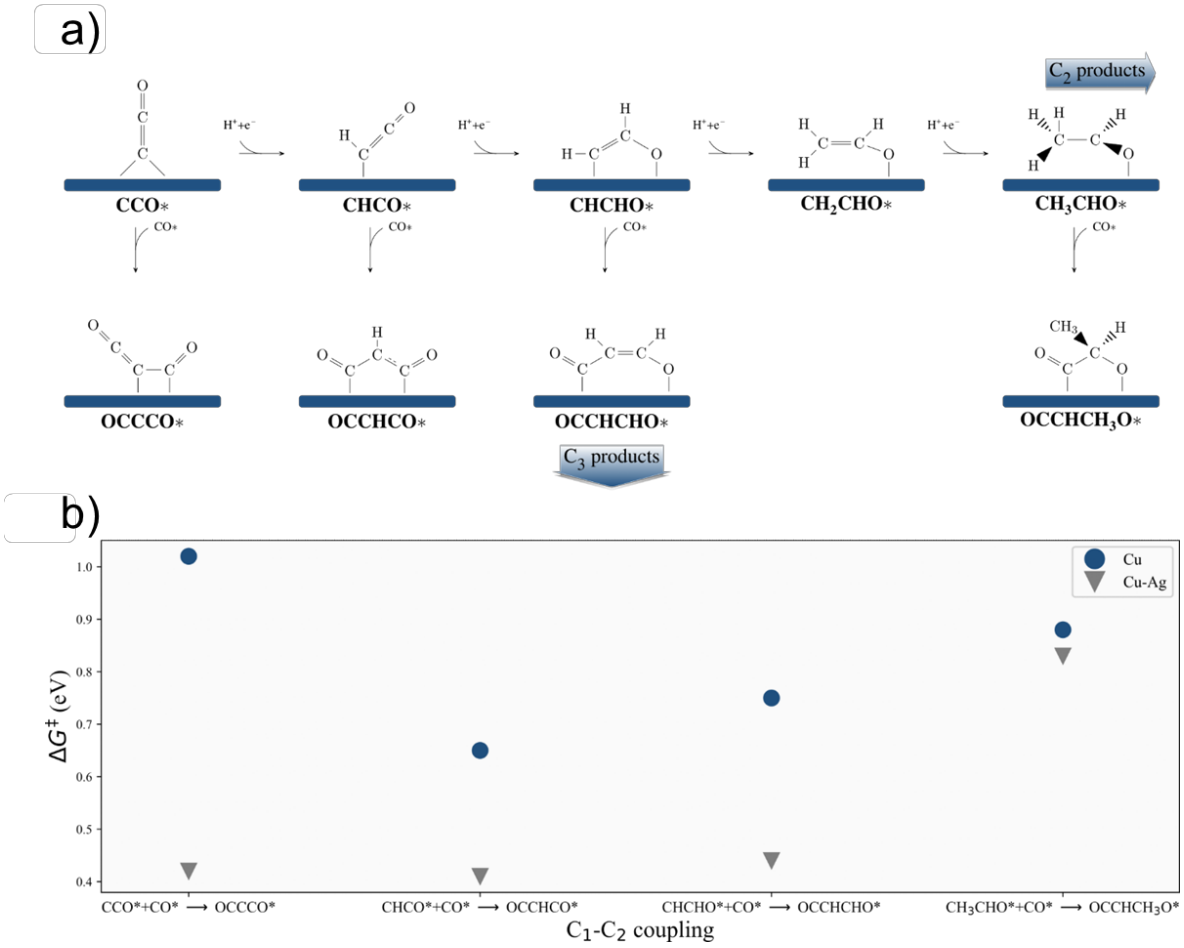

Figure 6. a) Selected elementary steps of the mechanism for the reduction of CO to C_2 and C_3 products on Cu(100) and Ag-doped Cu(100). b) Calculated free energy difference between the transition state and the initial state ($\Delta G^{\ddagger}$) for the selected C_1-C_2 coupling steps on Cu(100) and Ag-doped Cu(100).

In the proposed reaction mechanism, surface C_2 intermediates evolve either via proton coupled electron transfer (PCET) or by coupling to CO∗ (∗ is used to denote an adsorbed species) (Figure 6a). In line with previous studies,[10, 14-15] the successive PCET reactions from the CCO∗ species lead to the formation of CHCO∗, CHCHO∗, CH_2CHO∗ and CH_3CHO∗, with the latter being a precursor towards the formation of ethanol after 2 further PCETs. Each of these C_2 intermediates can undergo a coupling reaction with CO∗ to form different C_3 surface intermediates that in further steps can lead to the formation of C_3 products such as propanol. In agreement with previous studies,[15] the coupling between CH_2CHO∗ and CO∗ does not result in a stable C_3 surface species, hence this coupling reaction has been discarded (see Supplementary Information, section 4.5.4).

This article is protected by copyright. All rights reserved.

15213773, ja, Downloaded from https://onlinelibrary.wiley.com/doi/10.1002/anie.202310788 by Sorbonne Universite, Wiley Online Library on [16/10/2023]. See the Terms and Conditions (https://onlinelibrary.wiley.com/terms-and-conditions) on Wiley Online Library for rules of use; OA articles are governed by the applicable Creative Commons License

Accepted Manuscript

15213773, ja, Downloaded from https://onlinelibrary.wiley.com/doi/10.1002/anie.202310788 by Sorbonne Universite, Wiley Online Library on [16/10/2023]. See the Terms and Conditions (https://onlinelibrary.wiley.com/terms-and-conditions) on Wiley Online Library for rules of use; OA articles are governed by the applicable Creative Commons License

Accepted Manuscript

Furthermore, while CHCO∗ can be converted into another C2 intermediates (Figure S30), (namely CHCOH∗, coupling the latter with CO∗[9, 13] has been omitted since it has been reported to be only feasible on highly stepped surfaces such as Cu(511), where local field stabilizations can play a major role on the stability of that surface species[13] (in this study, the surface Cu(511) has not been detected experimentally). Finally, CHCO∗ can be converted into a physisorbed CH_2CO species which can react either with HO^-/H_2O forming acetate/acetic acid (experimental evidence has shown that this path is not being modified by the presence of Ag hence its study has been omitted) or in a PCET reaction leading to acetaldehyde, whose coupling with CO∗ is already considered in this study.[9]

The calculated transition state free energy barriers ($\Delta G^{\ddagger}$) are shown on Figure 6b. They show significant changes when Ag is added as a doping agent. In all cases, the reactions became more favorable for the Ag-doped system, with decrements of up to 0.24 eV for the free energy of reaction and up to 0.60 eV for the free energy barriers, in comparison with the Cu system. In line with previous studies,[6c, 14] these changes can be attributed to the interaction of the adsorbate with the different asymmetric Cu atoms of the Ag-doped surface, which leads to a stabilization of the surface C_3 species and of the corresponding transition state, thus decreasing the energetic barrier for the C_1-C_2 coupling. Although previous studies have suggested that the stability of the initial states can also be affected by creating less stable and hence more reactive species on the surface,[6c] this effect has not been observed in this work since the energetics of the initial states remain unchanged (Figure S31). The observed stabilization effect depends on the structure of the C_3 surface intermediate as well as on the number of surface asymmetric Cu atoms that interact with it. For instance, the largest stabilization effect occurs in the case of the CCO∗ + CO∗ coupling reaction, where the electronic structures of the unsaturated OCCCO∗ and of the transition state are more prone to be stabilized by the available electrons of the surface,. In contrast, the lowest stabilization effect was found for the CH_3CHO∗ + CO∗ coupling reaction, where the involved species are saturated and the $OCCHCH_3O$∗ species interacts with less asymmetric Cu atoms, since the CH_3 group is perpendicular to the surface thus resulting in an interaction similar to the one observed with the CHCHO∗ species. On the other hand, in the case of reduction of CCO∗ to CH_3CHO∗, the calculated free energies for each PCET step show negligible changes (less than 0.05 eV) when Cu is doped with Ag as compared to Cu (Figure S31).

This article is protected by copyright. All rights reserved.

15213773, ja, Downloaded from https://onlinelibrary.wiley.com/doi/10.1002/anie.202310788 by Sorbonne Universite, Wiley Online Library on [16/10/2023]. See the Terms and Conditions (https://onlinelibrary.wiley.com/terms-and-conditions) on Wiley Online Library for rules of use; OA articles are governed by the applicable Creative Commons License

Accepted Manuscript

As a result, based on the calculated energy barriers, it can be assumed that the addition of Ag as doping agent on Cu(100) has a positive effect on the C_1-C_2 coupling reactions in line with the experimental observations and previous studies on Cu(111).[6c]

Discussion

Thanks to an original cathode material, $CuAg_{5\%}N_{20h}$, consisting of Cu_3N/Cu doped with homogeneously dispersed Ag, and reaction conditions optimization, the highest Faradic Efficiency (FE) value for n-propanol ($FE_{C_3H_8O}$ = 45 %) reported so far (Table S2) has been obtained during electroreduction of CO, at high current density (150 mA cm^{-2}). In addition, to the best of our knowledge, the selectivity for liquid products (FE= 80 %) is among the highest reported to date for both CO_2R and COR at an industrially viable rate (150 mA cm^{-2}).[16] While doping Cu with Ag or Au has been previously used as a general strategy to favor ethanol production from CO_2 reduction,[17] such bimetallic materials have been very rarely studied for CO reduction.[6c, 6d, 16] Two recent studies actually showed that Ag-doped Cu slightly promotes n-propanol formation ($FE_{C_3H_8O}$ increased from 22% to 33% by a factor of 1.5 with respect to pristine Cu nanoparticles) with a further increase in the $FE_{C_3H_8O}$ value, by a factor of 1.1, by extra doping with Ru, to reach 36%.[6c, 6d] Here we report that combining Ag-doping with Cu nitridation provides a much larger effect on propanol formation from CO with $FE_{C_3H_8O}$ increasing by a factor of about 3.5. Few studies used Cu_3N as an electrocatalyst mostly for CO_2 electroreduction and in general they report a mixture of products, most often with ethylene as the major product and little n-propanol.[18] To our knowledge, only one study reported high Faradic efficiency for C_{2+} products (mainly ethylene and ethanol) during CO reduction using Cu_3N but n-propanol remained low (< 15%).[19] In one case Cu_3N has been associated with another metal species (In_2O_3) giving CO as the major product (FE_{CO} = 80%).[20]

Understanding the combined effect of Ag-doping and nitridation on Cu activity would be key for further optimization of catalysts for CO reduction to n-propanol. A clear outcome of the study reported here is that $CuAg_{5\%}N_{20h}$ is a precatalyst since, based on LSV and XPS, as well as on XRD and XANES *ex-situ* and *in-situ* characterization, we established that, under the cathodic potentials requested for catalysis, Cu_3N is converted to Cu^0. This is consistent with previous reports.[18a, 20] Another *operando* X-ray absorption spectroscopy (XAS) study clearly showed that Cu(I) from Cu_3N converts into Cu^0 during electroreduction.[19] As a consequence, the catalytically active species are likely nitride-derived metallic Cu^0 sites. However, the reactivity of these sites is clearly different from that of Cu^0 ones derived from pristine Cu

This article is protected by copyright. All rights reserved.

15213773, ja, Downloaded from https://onlinelibrary.wiley.com/doi/10.1002/anie.202310788 by Sorbonne Universite, Wiley Online Library on [16/10/2023]. See the Terms and Conditions (https://onlinelibrary.wiley.com/terms-and-conditions) on Wiley Online Library for rules of use; OA articles are governed by the applicable Creative Commons License

Accepted Manuscript

nanoparticles as well as from oxide-derived Cu^0 (OD-Cu) ones: indeed, different product distributions were obtained from CO reduction using these three classes of Cu^0 sites. However, it is difficult, at this stage, to have a clear view of how the local structure, the coordination and the electronic properties of nitride-derived Cu^0 sites are unique and differ from the others. As far as OD-Cu is concerned, after it was discovered as an outstanding catalyst, notably for CO reduction to ethanol,[6g] a large amount of studies suggested an important role of a variety of parameters such as grain boundaries, undercoordinated sites, subsurface oxygen, exposed facet, atomic defects, etc.[21] However, still, the current understanding of the actual active sites at the atomic level remains a challenging issue and continues to be under debate. Similarly, more studies will be needed for understanding the specific surface features of nitride-derived Cu^0 sites.

The increased roughness and porosity, thanks to the combination of Ag-doping and nitridation, as shown by microscopy, ECSA and BET measurements, is consistent with $CuAg_{5\%}N_{20h}$ providing the highest FE values for C_{2+} oxygenates. Previous reports have already shown that a high roughness factor or ECSA promotes selectivity for multicarbon oxygenates from CO.[6f-h] Indeed, a high density of accessible active sites and a high porosity favor CO penetration, CO coverage and C-C coupling reactions. As a matter of fact, liquid n-propanol formation rate (partial current density) reported here scales with the ESCA of the electrode.

Another remarkable characteristic of $CuAg_{5\%}N_{20h}$ resides in its sensitivity to KOH concentration, in terms of selectivity of CO reduction to liquid products. As far as acetate is concerned, a clear trend was observed in which $FE_{C_2H_4O_2}$ increases as a function of KOH concentration, up to 29% (Figure 3b). That acetate formation is favored under highly alkaline conditions is well established.[2b, 22] As supported by previous DFT calculations, this occurs via an ethenone intermediate which reacts with HO^- generating acetate.[22a-c] Decreasing the alkalinity, as expected, instead favors further coupled electron-proton transfers towards more reduced intermediates, precursors of ethanol and propanol. The highest $FE_{C_2H_6O}$ values were here obtained at the lowest alkalinity while the highest $FE_{C_3H_8O}$ values were obtained at intermediate alkalinity (1M KOH).

Propanol formation from CO is a greatly complicated reaction as it implies the transfer of 12 electrons and 12 protons as well as the formation of C_2-C_1 bonds and thus a very large number of possible intermediates, with short surface lifetime and low coverage. Since until now only little n-propanol formation was observed in CO_2/CO electrolysis in general, the

This article is protected by copyright. All rights reserved.

15213773, ja, Downloaded from https://onlinelibrary.wiley.com/doi/10.1002/anie.202310788 by Sorbonne Universite, Wiley Online Library on [16/10/2023]. See the Terms and Conditions (https://onlinelibrary.wiley.com/terms-and-conditions) on Wiley Online Library for rules of use; OA articles are governed by the applicable Creative Commons License

Accepted Manuscript

mechanism of CO conversion to n-propanol has been rarely studied and most computational investigations suggest that n-propanol should be produced via the coupling of a C_2 intermediate and an adsorbed CO.[15, 23] While the nature of this C_2 intermediate is unknown, we carried out a computational study, based on the computed most stable C_2 intermediates on Cu (100), following the conclusions of a previous report,[15] and here clearly establish that the presence of Ag on Cu results in a large decrease of activation barriers of C_2-CO coupling reactions leading to propanol, in full agreement with the experimental results.

Conclusion

We have reported a new class of Cu-based catalysts with record selectivity for n-propanol formation from CO electroreduction. The active Cu sites are Cu° atoms derived from Cu_3N and their selectivity for n-propanol is promoted by Ag doping. This opens new research directions towards selective catalysts for C_3 products formation via the exploration of a variety of metal-doped CuX (X= heteroatom) precursors and a better understanding of how such C_3 compounds can be accessible, as this would be the next step towards products with even longer chains.

Acknowledgements.

This work was financially supported by TotalEnergies SE. The authors thank Kevin Gako for their contribution to BET analysis. The *in-situ* XAS experiments at SAMBA beamline of Synchrotron SOLEIL have been funded by SOLEIL as the User Proposal 20221501 and by the European Research Council (ERC) Consolidator Grant GENESIS under the European Union's Horizon 2020 research and innovation program (grant agreement n° 864850).

Author contributions.

H.P.D. and N.H.T. contributed to the design of experiments and to acquisition and analysis of data; N.H.T., M.W.S. and M.F. contributed to the conception and design of the work; N.M performed TEM and XEDS analyses; M.W. performed EELS measurements., J.L performed the *in*-situ XRD experiments; D.V.P., D.P. and A.Z. performed the *ex-situ* and *in-situ* XAS experiments, S. Z. performed the XPS analysis; J.G.R.C. achieved the computation work; N.H.T. and M.F. have drafted the work, and M.W.S substantively revised it.

This article is protected by copyright. All rights reserved.

15213773, ja, Downloaded from https://onlinelibrary.wiley.com/doi/10.1002/anie.202310788 by Sorbonne Universite, Wiley Online Library on [16/10/2023]. See the Terms and Conditions (https://onlinelibrary.wiley.com/terms-and-conditions) on Wiley Online Library for rules of use; OA articles are governed by the applicable Creative Commons License

Accepted Manuscript

Keywords

Nitride derived CuAg catalyst, bimetallic CuAg, CO electroreduction, flow electrolyzer

Competing interests :

Authors declare that they have no competing interests.

Data availability:

All data are available in the main text or the Supplementary Information.

References

[1] a) S. Nitopi, E. Bertheussen, S. B. Scott, X. Liu, A. K. Engstfeld, S. Horch, B. Seger, I. E. L. Stephens, K. Chan, C. Hahn, J. K. Nørskov, T. F. Jaramillo, I. Chorkendorff, *Chemical Reviews* **2019**, *119*, 7610-7672; b) P. De Luna, C. Hahn, D. Higgins, S. A. Jaffer, T. F. Jaramillo, E. H. Sargent, *Science* **2019**, *364*, eaav3506.

[2] a) D. Wakerley, S. Lamaison, J. Wicks, A. Clemens, J. Feaster, D. Corral, S. A. Jaffer, A. Sarkar, M. Fontecave, E. B. Duoss, S. Baker, E. H. Sargent, T. F. Jaramillo, C. Hahn, *Nature Energy* **2022**, *7*, 130-143; b) M. Jouny, G. S. Hutchings, F. Jiao, *Nature Catalysis* **2019**, *2*, 1062-1070; c) D. M. Weekes, D. A. Salvatore, A. Reyes, A. Huang, C. P. Berlinguette, *Accounts of Chemical Research* **2018**, *51*, 910-918.

[3] a) C. Chen, Y. Li, P. Yang, *Joule* **2021**, *5*, 737-742; b) M. Ma, E. L. Clark, K. T. Therkildsen, S. Dalsgaard, I. Chorkendorff, B. Seger, *Energy & Environmental Science* **2020**, *13*, 977-985; c) J. A. Rabinowitz, M. W. Kanan, *Nature Communications* **2020**, *11*, 5231; d) N. S. Romero Cuellar, K. Wiesner-Fleischer, M. Fleischer, A. Rucki, O. Hinrichsen, *Electrochimica Acta* **2019**, *307*, 164-175.

[4] a) J. E. Huang, F. Li, A. Ozden, A. Sedighian Rasouli, F. P. García de Arquer, S. Liu, S. Zhang, M. Luo, X. Wang, Y. Lum, Y. Xu, K. Bertens, R. K. Miao, C.-T. Dinh, D. Sinton, E. H. Sargent, *Science* **2021**, *372*, 1074-1078; b) J. Gu, S. Liu, W. Ni, W. Ren, S. Haussener, X. Hu, *Nature Catalysis* **2022**, *5*, 268-276; c) A. Perazio, C. E. Creissen, J. G. Rivera de la Cruz, M. W. Schreiber, M. Fontecave, *ACS Energy Letters* **2023**, *8*, 2979-2985.

[5] a) A. Ozden, Y. Wang, F. Li, M. Luo, J. Sisler, A. Thevenon, A. Rosas-Hernández, T. Burdyny, Y. Lum, H. Yadegari, T. Agapie, J. C. Peters, E. H. Sargent, D. Sinton, *Joule* **2021**, *5*, 706-719; b) J. Sisler, S. Khan, A. H. Ip, M. W. Schreiber, S. A. Jaffer, E. R. Bobicki, C.-T. Dinh, E. H. Sargent, *ACS Energy Letters* **2021**, *6*, 997-1002; c) R. Chen, H.-Y. Su, D. Liu, R. Huang, X. Meng, X. Cui, Z.-Q. Tian, D. H. Zhang, D. Deng, *Angewandte Chemie International Edition* **2020**, *59*, 154-160.

[6] a) N.-H. Tran, H. P. Duong, G. Rousse, S. Zanna, M. W. Schreiber, M. Fontecave, *ACS Applied Materials & Interfaces* **2022**, *14*, 31933-31941; b) H. P. Duong, N.-H. Tran, G. Rousse, S. Zanna, M. W. Schreiber, M. Fontecave, *ACS Catalysis* **2022**, *12*, 10285-10293; c) X. Wang, Z. Wang, T.-T. Zhuang, C.-T. Dinh, J. Li, D.-H. Nam, F. Li, C.-W. Huang, C.-S. Tan, Z. Chen, M. Chi, C. M. Gabardo, A. Seifitokaldani, P. Todorović, A. Proppe, Y. Pang, A. R. Kirmani, Y. Wang, A. H. Ip, L. J. Richter, B. Scheffel, A. Xu, S.-C. Lo, S. O. Kelley, D. Sinton, E. H. Sargent, *Nature Communications* **2019**, *10*, 5186; d) X. Wang, P. Ou, A. Ozden, S.-F. Hung, J. Tam, C. M. Gabardo, J. Y. Howe, J. Sisler, K. Bertens, F. P. García de Arquer, R. K. Miao, C. P. O'Brien, Z.

This article is protected by copyright. All rights reserved.

Wang, J. Abed, A. S. Rasouli, M. Sun, A. H. Ip, D. Sinton, E. H. Sargent, *Nature Energy* **2022**, *7*, 170-176; e) J. Li, Z. Wang, C. McCallum, Y. Xu, F. Li, Y. Wang, C. M. Gabardo, C.-T. Dinh, T.-T. Zhuang, L. Wang, J. Y. Howe, Y. Ren, E. H. Sargent, D. Sinton, *Nature Catalysis* **2019**, *2*, 1124-1131; f) D. Raciti, L. Cao, K. J. T. Livi, P. F. Rottmann, X. Tang, C. Li, Z. Hicks, K. H. Bowen, K. J. Hemker, T. Mueller, C. Wang, *ACS Catalysis* **2017**, *7*, 4467-4472; g) C. W. Li, J. Ciston, M. W. Kanan, *Nature* **2014**, *508*, 504-507; h) L. Wang, S. Nitopi, A. B. Wong, J. L. Snider, A. C. Nielander, C. G. Morales-Guio, M. Orazov, D. C. Higgins, C. Hahn, T. F. Jaramillo, *Nature Catalysis* **2019**, *2*, 702-708; i) M. Jouny, W. Luc, F. Jiao, *Nature Catalysis* **2018**, *1*, 748-755; j) Z. Gu, H. Shen, Z. Chen, Y. Yang, C. Yang, Y. Ji, Y. Wang, C. Zhu, J. Liu, J. Li, T.-K. Sham, X. Xu, G. Zheng, *Joule* **2021**, *5*, 429-440; k) Q. Lei, H. Zhu, K. Song, N. Wei, L. Liu, D. Zhang, J. Yin, X. Dong, K. Yao, N. Wang, X. Li, B. Davaasuren, J. Wang, Y. Han, *Journal of the American Chemical Society* **2020**, *142*, 4213-4222; l) D. S. Ripatti, T. R. Veltman, M. W. Kanan, *Joule* **2019**, *3*, 240-256.

[7] M. Jouny, W. Luc, F. Jiao, *Industrial & Engineering Chemistry Research* **2018**, *57*, 2165-2177.

[8] A. Miura, T. Takei, N. Kumada, *Journal of Asian Ceramic Societies* **2014**, *2*, 326-328.

[9] A. H. M. da Silva, Q. Lenne, R. E. Vos, M. T. M. Koper, *ACS Catalysis* **2023**, *13*, 4339-4347.

[10] H.-J. Peng, M. T. Tang, J. Halldin Stenlid, X. Liu, F. Abild-Pedersen, *Nature Communications* **2022**, *13*, 1399.

[11] a) J. Resasco, L. D. Chen, E. Clark, C. Tsai, C. Hahn, T. F. Jaramillo, K. Chan, A. T. Bell, *Journal of the American Chemical Society* **2017**, *139*, 11277-11287; b) S. Ringe, E. L. Clark, J. Resasco, A. Walton, B. Seger, A. T. Bell, K. Chan, *Energy & Environmental Science* **2019**, *12*, 3001-3014.

[12] Y. F. Nishimura, H.-J. Peng, S. Nitopi, M. Bajdich, L. Wang, C. G. Morales-Guio, F. Abild-Pedersen, T. F. Jaramillo, C. Hahn, *ACS Applied Materials & Interfaces* **2021**, *13*, 52044-52054.

[13] H. Xiao, W. A. Goddard, T. Cheng, Y. Liu, *Proceedings of the National Academy of Sciences* **2017**, *114*, 6685-6688.

[14] H. Peng, M. T. Tang, X. Liu, P. Schlexer Lamoureux, M. Bajdich, F. Abild-Pedersen, *Energy & Environmental Science* **2021**, *14*, 473-482.

[15] M. T. Tang, H.-J. Peng, J. H. Stenlid, F. Abild-Pedersen, *The Journal of Physical Chemistry C* **2021**, *125*, 26437-26447.

[16] J. Li, H. Xiong, X. Liu, D. Wu, D. Su, B. Xu, Q. Lu, *Nature Communications* **2023**, *14*, 698.

[17] a) P. Wang, H. Yang, C. Tang, Y. Wu, Y. Zheng, T. Cheng, K. Davey, X. Huang, S.-Z. Qiao, *Nature Communications* **2022**, *13*, 3754; b) C. G. Morales-Guio, E. R. Cave, S. A. Nitopi, J. T. Feaster, L. Wang, K. P. Kuhl, A. Jackson, N. C. Johnson, D. N. Abram, T. Hatsukade, C. Hahn, T. F. Jaramillo, *Nature Catalysis* **2018**, *1*, 764-771; c) D. Karapinar, C. E. Creissen, J. G. Rivera de la Cruz, M. W. Schreiber, M. Fontecave, *ACS Energy Letters* **2021**, *6*, 694-706; d) S. Kuang, Y. Su, M. Li, H. Liu, H. Chuai, X. Chen, E. J. M. Hensen, T. J. Meyer, S. Zhang, X. Ma, *Proceedings of the National Academy of Sciences* **2023**, *120*, e) 2214175120; eY. C. Li, Z. Wang, T. Yuan, D.-H. Nam, M. Luo, J. Wicks, B. Chen, J. Li, F. Li, F. P. G. de Arquer, Y. Wang, C.-T. Dinh, O. Voznyy, D. Sinton, E. H. Sargent, *Journal of the American Chemical Society* **2019**, *141*, 8584-8591; f) Y. Lum, J. W. Ager, *Energy & Environmental Science* **2018**, *11*, 2935-2944; g) C. Chen, Y. Li, S. Yu, S. Louisia, J. Jin, M. Li, M. B. Ross, P. Yang, *Joule* **2020**, *4*, 1688-1699.

[18] a) M. Ebaid, K. Jiang, Z. Zhang, W. S. Drisdell, A. T. Bell, J. K. Cooper, *Chemistry of Materials* **2020**, *32*, 3304-3311; b) Z. Yin, C. Yu, Z. Zhao, X. Guo, M. Shen, N. Li, M. Muzzio, J. Li, H. Liu, H. Lin, J. Yin, G. Lu, D. Su, S. Sun, *Nano Letters* **2019**, *19*, 8658-8663; c) M. Zheng, P. Wang, X. Zhi, K. Yang, Y. Jiao, J. Duan, Y. Zheng, S.-Z. Qiao, *Journal of the American Chemical Society* **2022**, *144*, 14936-14944.

[19] C. Zhao, G. Luo, X. Liu, W. Zhang, Z. Li, Q. Xu, Q. Zhang, H. Wang, D. Li, F. Zhou, Y. Qu, X. Han, Z. Zhu, G. Wu, J. Wang, J. Zhu, T. Yao, Y. Li, H. J. M. Bouwmeester, Y. Wu, *Advanced Materials* **2020**, *32*, 2002382.

[20] F. L. P. Veenstra, A. J. Martín, J. Pérez-Ramírez, *ChemSusChem* **2019**, *12*, 3501-3508.

[21] a) D. Cheng, Z.-J. Zhao, G. Zhang, P. Yang, L. Li, H. Gao, S. Liu, X. Chang, S. Chen, T. Wang, G. A. Ozin, Z. Liu, J. Gong, *Nature Communications* **2021**, *12*, 395; b) Y. Lum, J. W. Ager, *Nature Catalysis* **2019**, *2*, 86-93; c) A. Eilert, F. Cavalca, F. S. Roberts, J. Osterwalder, C. Liu, M. Favaro,

This article is protected by copyright. All rights reserved.

15213773, ja, Downloaded from https://onlinelibrary.wiley.com/doi/10.1002/anie.202310788 by Sorbonne Universite, Wiley Online Library on [16/10/2023]. See the Terms and Conditions (https://onlinelibrary.wiley.com/terms-and-conditions) on Wiley Online Library for rules of use; OA articles are governed by the applicable Creative Commons License

Accepted Manuscript

E. J. Crumlin, H. Ogasawara, D. Friebel, L. G. M. Pettersson, A. Nilsson, *The Journal of Physical Chemistry Letters* **2017**, *8*, 285-290; d) X. Feng, K. Jiang, S. Fan, M. W. Kanan, *ACS Central Science* **2016**, *2*, 169-174; e) A. Verdaguer-Casadevall, C. W. Li, T. P. Johansson, S. B. Scott, J. T. McKeown, M. Kumar, I. E. L. Stephens, M. W. Kanan, I. Chorkendorff, *Journal of the American Chemical Society* **2015**, *137*, 9808-9811; f) C. Chen, X. Yan, Y. Wu, S. Liu, X. Sun, Q. Zhu, R. Feng, T. Wu, Q. Qian, H. Liu, L. Zheng, J. Zhang, B. Han, *Chemical Science* **2021**, *12*, 5938-5943.

[22] a) H. H. Heenen, H. Shin, G. Kastlunger, S. Overa, J. A. Gauthier, F. Jiao, K. Chan, *Energy & Environmental Science* **2022**, *15*, 3978-3990; b) M. Ma, W. Deng, A. Xu, D. Hochfilzer, Y. Qiao, K. Chan, I. Chorkendorff, B. Seger, *Energy & Environmental Science* **2022**, *15*, 2470-2478; c) W. Luc, X. Fu, J. Shi, J.-J. Lv, M. Jouny, B. H. Ko, Y. Xu, Q. Tu, X. Hu, J. Wu, Q. Yue, Y. Liu, F. Jiao, Y. Kang, *Nature Catalysis* **2019**, *2*, 423-430; d) H. Xiao, T. Cheng, W. A. Goddard, III, R. Sundararaman, *Journal of the American Chemical Society* **2016**, *138*, 483-486.

[23] S. Pablo-García, F. L. P. Veenstra, L. R. L. Ting, R. García-Muelas, F. Dattila, A. J. Martín, B. S. Yeo, J. Pérez-Ramírez, N. López, *Catalysis Science & Technology* **2022**, *12*, 409-417.

This article is protected by copyright. All rights reserved.

15213773, ja, Downloaded from https://onlinelibrary.wiley.com/doi/10.1002/anie.202310788 by Sorbonne Universite, Wiley Online Library on [16/10/2023]. See the Terms and Conditions (https://onlinelibrary.wiley.com/terms-and-conditions) on Wiley Online Library for rules of use; OA articles are governed by the applicable Creative Commons License

Accepted Manuscript

10.1002/anie.202310788

TOC figure

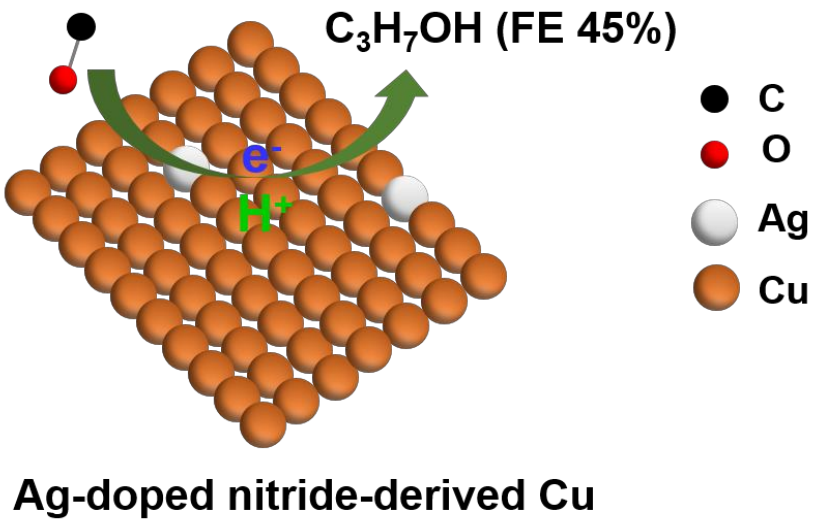

Ag-doped nitride-derived Cu

Ag-doped copper nitride is a highly selective electrocatalyst for CO reduction to n-propanol leading to a record Faradic Efficiency value of 45% at an industrially-relevant current density of 150 mA cm^{-2}, in an alkaline flow electrolyser.

This article is protected by copyright. All rights reserved.

15213773, ja, Downloaded from https://onlinelibrary.wiley.com/doi/10.1002/anie.202310788 by Sorbonne Universite, Wiley Online Library on [16/10/2023]. See the Terms and Conditions (https://onlinelibrary.wiley.com/terms-and-conditions) on Wiley Online Library for rules of use; OA articles are governed by the applicable Creative Commons License

Accepted Manuscript